This is a peer-reviewed, accepted author manuscript of the following article: Capdevila-Echeverria, J., Wang, J., Lakerveld, R., & ter Horst, J. H. (2021). Process modeling and optimization of continuous chiral resolution by integration of membrane and crystallization technologies. Journal of Membrane Science, 632, [119359]. https://doi.org/10.1016/j.memsci.2021.119359

Process modeling and optimization of continuous chiral resolution by integration of membrane and crystallization technologies

Jose Capdevila-Echeverria[a,*], Jiayuan Wang[b], Richard Lakerveld[b], Joop H. ter Horst[a,*]

[a] EPSRC Future Manufacturing Hub for Continuous Manufacture and Advanced Crystallisation (CMAC), Strathclyde Institute of Pharmacy and Biomedical Sciences (SIPBS), Technology and Innovation Centre, University of Strathclyde, 99 George Street, Glasgow G1 1RD, United Kingdom

[b] Department of Chemical and Biological Engineering, The Hong Kong University of Science and Technology, Clear Water Bay, Hong Kong

* Corresponding authors. E-mail addresses:

jose.capdevila-echeverria@strath.ac.uk, joop.terhorst@strath.ac.uk

Abstract

Chiral resolution will increase its importance in the pharmaceutical, pesticide, and food industries since future chiral products will be structurally more complex while their quality will need to meet stringent demands to accomplish with health, crop, and environmental purposes. Currently, obtaining enantiopure crystals from racemic compound-forming systems (90-95% of chiral compounds) remains a challenge. The combination of membrane ultrafiltration and crystallization in a continuous process is a potential solution to this problem. This work aims to optimize this continuous chiral resolution process using process modeling. First, a model for the membrane ultrafiltration step assumes a one-site competition in which the chiral selector binds preferentially to one of the enantiomers. The amino acids phenylalanine, alanine, and valine in aqueous media along with the chiral selector BSA are the model systems studied. Then, three process performance parameters (purity, recovery, and a combination of the previous two) are assessed to optimize the conditions for the continuous membrane-based step. Recoveries up to 70% are achieved while fulfilling purity levels beyond eutectic point compositions, a requirement for the enantiopure crystallization. Additionally, the properties of an ideal process chiral selector are explored. Finally, the crystallization step (with recoveries up to 65%) is coupled to evaluate the maximum recovery of the overall process. Simulations show that the membrane-crystallization process performance is governed by a trade-off between purity and recovery. We predict that an ideal BSA-similar chiral selector should bear an unprotonated binding site for a wide pH range and a difference between enantiomer complexation constants of at least 2-3 *pK* units to improve the process performance.

Keywords: chiral separation, continuous process, membrane, crystallization, process modeling

1. Introduction

Chiral molecules occur in left- and right-handed configurations that can be considered as mirror images (enantiomers), and that, like hands, cannot be superimposed onto each other [1]. Enantiomers of chiral drugs may present different pharmacological and toxicological effects [1,2]. For instance, the (*S*)-enantiomer of naproxen when administered in the human body has an anti-inflammatory effect whereas the (*R*)-enantiomer is poisonous to the liver [3,4]. In the absence of in vivo racemization, chiral resolution (the process to obtain enantiopure molecules by means of the physical separation of enantiomers) of racemic mixtures or impure enantiomers would prevent the undesired effects. Chiral resolution processes are therefore of great importance in the pharmaceutical industry as well as in the agrochemical and food manufacturing sectors [5–7]. The chiral separation of racemic environmental pollutants has also attracted attention due to the different impact of each enantiomer to the environment [8,9]. The chiral pollution is a serious issue for health and environment due to the enantioselective biodegradation of the chiral pollutants. More than 1500 chiral pollutants are present in the environment [10]. Chiral resolution will increase its already sizeable importance in these fields where future chemical products will be larger and contain more stereocenters while their quality and purity will require to meet increasingly stringent demands and specifications. However, the separation of enantiomers into highly enantiopure crystalline products from a complex multicomponent mixture remains a challenge.

Although continuous membrane technologies could potentially be used to achieve enantiomer enrichment, they cannot reach enantiomer purity levels close to 100% in a feasible manner. The consecution of high purity would require several membranes, a fact that would compromise the recovery of the process, and therefore making the process unfeasible [11]. Some efforts have been done in obtaining high purity levels in solution, but none of them led

to the full separation and neither to the recovery of a pure solid product [12–14]. While crystallization-enabled resolution such as preferential crystallization can be highly effective and efficient due to the near-perfect selectivity of the solid phase, it relies on the formation of a conglomerate [5,6]. Nonetheless, in racemic solutions, only 5-10% of the chiral compounds form such conglomerates while the majority of the chiral compounds (90-95%) form a racemic compound [5,6,15–19]. Therefore, obtaining enantiopure crystalline products from racemic solutions of racemic compounds is currently a challenge.

Integrated processes can combine the high productivity of a not too selective separation technology with a narrow process window but highly selective separation technology. The first technology is used to create the conditions with the right process window for the second technology. Here, the selectivity is understood in terms of the required enantiomeric enrichment that the first technology will be able to provide to the second technology, which will produce the enantiopure products. Examples of these integrated processes are pertraction-crystallization [20,21] and chromatography-crystallization [22,23]. A third novel approach is to couple membrane ultrafiltration and crystallization processes, so forming a membrane ultrafiltration-crystallization integrated process. In this latter, a chiral selector is used to preferentially complex one of the enantiomers. A membrane ultrafiltration process renders enantiomeric enrichment by means of a size-exclusion non-enantioselective solid membrane. This type of membranes is promising due to its convenience, affordability, energy efficiency, and ease of scale-up [11]. From the enriched solution, the enriched enantiomer can be selectively crystallized in the permeate as an enantiopure solid.

Here we report the process modeling and optimization of a continuous chiral resolution process that combines membrane ultrafiltration and cooling crystallization to produce enantiopure crystal products starting from racemic solutions of racemic compound-forming systems. The chiral systems chosen to demonstrate the feasibility of the membrane-assisted

crystallization resolution are the hydrophobic amino acids phenylalanine (Phe), alanine (Ala), and valine (Val) in aqueous media. Bovine serum albumin (BSA) is a chiral selector, which is known to have enantiomeric selectivity with this class of amino acids [12–14]. A one-site competition model is presented to describe the complexation interaction of these amino acids systems with the chiral selector BSA. The model is validated and its predictions determine the optimal conditions for the membrane process. In addition, sensitivity studies of thermodynamic constants permit the prediction of the ideal chiral selector properties. Finally, the feasibility of coupling the membrane ultrafiltration and crystallization is investigated.

2. Experimental section

2.1. Materials

D-phenylalanine (D-Phe, Sigma-Aldrich, ≥98%), L-phenylalanine (L-phe; Sigma-Aldrich, ≥99%), D-alanine (D-Ala, Sigma-Aldrich, ≥98%), L-alanine (L-ala; Sigma-Aldrich, ≥99%), D-valine (D-Val, Sigma-Aldrich, ≥98%), and L-valine (L-val; Sigma-Aldrich, ≥98%) were used as purchased. Milli-Q water was taken from a Merck Millipore purification system and had a resistivity of 18.2 MΩ·cm at 25ºC.

2.2. Solubility determination methodologies

Two different methods were used to determine the solubilities at temperatures T = 80ºC and T' = 1ºC because some systems present fouling phenomena when they crystallize, which prevented using light to detect the presence of crystals for some of the amino acid systems studied. A second gravimetric method based on equilibrium concentration was required to assess their solubilities. The two methods used were the temperature variation (TV) and equilibrium concentration (EqC) methods [24].

2.2.1. Temperature variation (TV) method

For the TV method, a similar protocol was used as reported in the literature [24] using the Crystal16 multiple reactor setup (Technobis Crystallization Systems). Samples were prepared by dissolving increasing amounts of the solid with 1 mL of Milli-Q water in each vial. The samples were agitated using a magnetic stirrer bar with a stirring rate of 700 rpm. Three temperature cycles were applied starting at 20ºC, with maximum and minimum temperatures of 90ºC and 1ºC, respectively, and with heating and cooling rates of 0.3 ºC/min. Hold times of 1 h were applied when maximum (90ºC) and minimum (1ºC) temperatures were reached in each cycle. Clear and cloud points were registered based on the transmission of the light. Then,

the solubility at a certain temperature was determined by taking the average of three clear points measurements (*RSD* within ±1%). This method was used for the solubility determination of alanine.

2.2.2. Equilibrium concentration (EqC) method

For the EqC method, a similar gravimetric protocol was used as reported in the literature [24]. Samples were prepared by adding an excess of compound to 1 mL of Milli-Q water in each vial. Then, the saturated solutions in the vials were equilibrated at different constant temperatures in the Crystal16 multiple reactor setup (Technobis Crystallization Systems) for at least 2-3 days. During that period, the samples were agitated using a magnetic stirrer bar with a stirring rate of 700 rpm. Afterwards, at various temperatures, solution samples of approximately 1 mL were taken with a syringe, filtered, weighed and left in the oven (65ºC) for at least 7 days for the solvent to evaporate. When the crystals appeared dry, they were weighed. Two days later, they were weighed again to check for any additional mass loss until the mass was constant. The solubility at a certain temperature was determined by taking the average of three gravimetric measurements (*RSD* within ±2%). This method was used for the solubility determination of phenylalanine and valine.

2.3. Computational software

The process model presented in this document was implemented in GAMS 24.7.4 [25] and all the optimization problems were solved using the GAMS/CONOPT solver, which is based on the generalized reduced gradient method and generally used for large-scale non-linear programming (NLP) optimization problems [26]. To avoid local optima, multiple initial guesses were provided by a random number generator in MATLAB R2018A [27] to GAMS using the GDXMRW interface [28].

3. Results

3.1. Model development

The novel chiral resolution process consists in an initial feed of a racemic amino acid aqueous solution which first undergoes an enantiomeric enrichment by means of a chiral selector-assisted membrane ultrafiltration step followed by selective crystallization of an enantiopure crystalline product (Fig. 1).

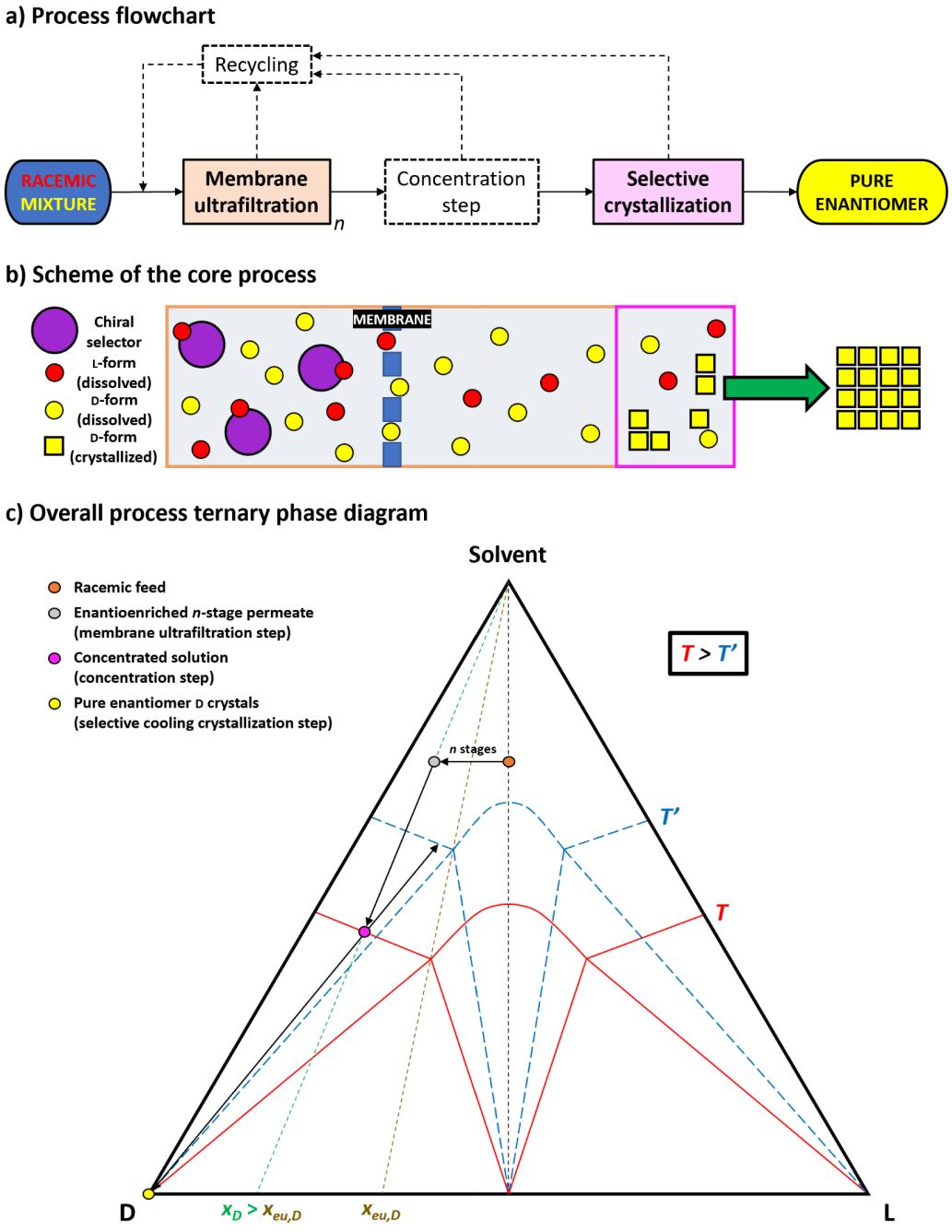

Fig. 1. a) Process flowchart for the membrane-crystallization chiral resolution. b) Scheme of the core process (colors relate to the core steps in bold in a). c) Overall process ternary phase diagram for the resolution of a racemic compound-forming system. *T* and *T'* account for both initial and final temperatures in the cooling crystallization step, respectively; and x_D and $x_{eu,D}$ are the solvent-free enantiomer fraction and eutectic point composition for enantiomer D, respectively.

3.1.1. Membrane ultrafiltration step

We assumed that the one-site competition model [12–14] explains the complexation between the chiral selector BSA and the enantiomers of hydrophobic amino acids phenylalanine (Phe), alanine (Ala), and valine (Val) in the membrane ultrafiltration step (Fig. 1). This one-site competition model was applied to systems with the similar amino acids tryptophan (Trp) and kynurenine, as reported by Garnier [13] and Randon [14]. The mechanism considers that only the zwitterionic forms of both enantiomers of the amino acid will compete to bind to a single unprotonated site of the chiral selector BSA (Fig. 1b).

In this way, this model accounts for the speciation found in the membrane ultrafiltration step (Fig. 1b) taking into consideration the combination of three thermodynamic equilibria:

1) Complexation equilibria of chiral selector BSA with the zwitterionic form of the amino acid enantiomers

$$\mathrm{D}^{\pm} + \mathrm{BSA} \rightleftharpoons \mathrm{D}^{\pm}\mathrm{BSA}, \quad K_D = \frac{C_{D\pm BSA}}{C_{D\pm} C_{BSA}} \tag{1a}$$

$$\mathrm{L}^{\pm} + \mathrm{BSA} \rightleftharpoons \mathrm{L}^{\pm}\mathrm{BSA}, \quad K_L = \frac{C_{L\pm BSA}}{C_{L\pm} C_{BSA}} \tag{1b}$$

K and *C* represent the thermodynamic constants and species concentrations involved in the complexation equilibria, respectively (see Notation section 4.6.). K_D and K_L should differ from each other as much as possible for the pair of enantiomers, indicating then a much higher

selectivity of the chiral selector for one of the two enantiomers. This difference is essential to obtain an enantiopure crystalline product at the end of the overall process (Fig. 1).

2) Acid-base dissociation equilibria of each amino acid enantiomer with solvent

$$\mathrm{D^+ + H_2O \rightleftharpoons D^{\pm} + H_3O^+},\ K_{a1,D} = \frac{C_{D\pm}C_{w+}}{C_{D+}C_w} \tag{2a}$$

$$\mathrm{D^{\pm} + H_2O \rightleftharpoons D^- + H_3O^+},\ K_{a2,D} = \frac{C_{D-}C_{w+}}{C_{D\pm}C_w} \tag{2b}$$

$$\mathrm{L^+ + H_2O \rightleftharpoons L^{\pm} + H_3O^+},\ K_{a1,L} = \frac{C_{L\pm}C_{w+}}{C_{L+}C_w} \tag{2c}$$

$$\mathrm{L^{\pm} + H_2O \rightleftharpoons L^- + H_3O^+},\ K_{a2,L} = \frac{C_{L-}C_{w+}}{C_{L\pm}C_w} \tag{2d}$$

K_a and C represent the thermodynamic constants and species concentrations involved in the acid-base dissociation equilibria, respectively (see Notation section 4.6.). Here, $K_{a1,D} = K_{a1,L}$ and $K_{a2,D} = K_{a2,L}$ because the acid-base dissociation thermodynamic equilibria are not affected by stereoisomerism.

3) Acid-base dissociation equilibrium of the chiral selector BSA with solvent

$$\mathrm{BSA^+ + H_2O \rightleftharpoons BSA + H_3O^+},\ K_{BSA} = \frac{C_{BSA}C_{w+}}{C_{BSA+}C_w} \tag{3}$$

K_{BSA} and C represent the thermodynamic constant and species concentrations involved in the acid-base dissociation equilibrium of BSA, respectively (see Notation section 4.6.). The values for the above thermodynamic constants are given in Table 1, indicated as pK (which means -$\log_{10}K$). The values of pK_D and pK_L for alanine and valine systems are assumed equal to those for phenylalanine [29] because of the similar hydrophobic amino acid behavior (Table 1). As mentioned above, acid-base dissociation constants, and then also pK_{a1} and pK_{a2}, have

the same values for both enantiomers [30]. The acid-base dissociation equilibrium of BSA with water is reported in the literature [13,14].

Table 1. pK values for thermodynamic equilibria constants in Eqs. (1)-(3) for the amino acid systems studied at 25ºC. pK_D and pK_L, pK_{a1} and pK_{a2}, and pK_{BSA} account for the complexation constants of both amino acid enantiomers with BSA and acid-base dissociation constants of the amino acid enantiomers and BSA with water, respectively.

Amino acid	pK_D	pK_L	pK_{a1}	pK_{a2}	pK_{BSA}
Phenylalanine			1.83	9.13	
Alanine	-5.27	-6.25	2.34	9.69	9.40
Valine			2.32	9.62	

The thermodynamic constants described above (Table 1) along with the material balances for each enantiomer of the amino acid and chiral selector permit the study of the speciation in the membrane ultrafiltration step (Fig. 1ab). The material balances considered for the different species x involved in this step can be expressed as follows (4):

$$C_{x,0} = \sum_{i \in species\ x\ forms} C_i \qquad (4)$$

Species x are enantiomer D or L or chiral selector BSA. $C_{x,0}$ and C_i represent the total concentration of species x and concentration for each form of species x present in the membrane ultrafiltration step, respectively.

The membrane ultrafiltration step consists of a filtration system which makes use of a size-exclusion non-stereoselective solid membrane. This membrane is assumed to have total rejection for the chiral selector and chiral selector-amino acid complexes. In that way, only the free enantiomers of the amino acids (D and L-forms) can permeate the membrane. The model membrane is also assumed to not influence the permeate concentration compared to the retentate solution which means that the free enantiomers concentrations in the retentate and permeate solutions are equal ($C_{D,r} = C_{D,p}$ and $C_{L,r} = C_{L,p}$). Only the retentate volume V_r and

permeate volume V_p vary over time. As the chiral selector, present at the retentate side of the membrane, preferentially binds one of the enantiomers, the permeate solution gets enantioenriched with the other (Fig. 1ab) [31,32]. In the amino acid systems treated here, the enantiomer L preferentially binds to the chiral selector and therefore the enantiomer D is enriched in the permeate (Fig. 1b), which can be seen from the higher complexation value of K_L (more negative pK) compared to K_D (less negative pK) (see Table 1). Several recirculation cycles of the retentate solution occur in the membrane ultrafiltration step to produce enough permeate volume V_p to go further in the next steps of the overall process at the end of the membrane step. That is, a certain volume V_p from the initial feed volume V_0 is collected at the permeate side. The enantiomeric enrichment level reached in the permeate solution can be increased if the number of membrane ultrafiltration stages n is also increased (Fig. 1a). This option can be used to optimize the process, meaning that the membrane ultrafiltration step can be adapted with more stages for chemical systems that require a higher enantiomeric enrichment. The model description in this section mainly refers to the single-stage membrane ultrafiltration (n = 1) case. Then, the two outgoing streams in the membrane ultrafiltration step (Fig. 1a) are taken as the retentate and permeate. The multi-stage membrane ultrafiltration (n > 1) case is treated with further detail in section 4.3.3. as an extended approach for those systems that require high enantioenrichment.

We define three key performance indicators (KPIs) to assess the performance of the membrane ultrafiltration step (Fig. 1ab) as defined below (5)-(7):

1) Purity of the membrane ultrafiltration step (for permeate stream, Table 2)

$$Pu_m = x_D = \frac{C_{D,p}}{C_{D,p} + C_{L,p}} \tag{5}$$

Purity Pu_m is defined by the solvent-free enantiomer D fraction x_D. $C_{D,p}$ and $C_{L,p}$ represent the total concentrations of enantiomers D and L in the permeate p, respectively.

2) Recovery of the membrane ultrafiltration step (Table 2)

$$Re_m = \frac{V_p C_{D,p}}{V_0 C_{D,0}} \tag{6}$$

$C_{D,0}$ represents the total initial concentration of enantiomer D in the feed solution.

3) *PuRe* of the membrane ultrafiltration step (Table 2)

$$PuRe = E_{D,p} Re_m = (2Pu_m - 1) Re_m \tag{7}$$

This *PuRe* definition can be inferred from Pu_m and Re_m alongside their relationship with the enantiomeric excess $E_{D,p}$ defined as:

$$E_{D,p} = \frac{C_{D,p} - C_{L,p}}{C_{D,p} + C_{L,p}} = x_D - x_L = 2Pu_m - 1 \tag{8}$$

Note that we use the fact that the total sum of both solvent-free enantiomer fractions for enantiomers D and L (x_D and x_L, respectively) is equal to 1.

The three KPIs defined for the membrane ultrafiltration step, indicated by the subscript m, are considered sufficient to study this step with a thermodynamic approach considering the equilibria and concentrations that involve the one-site competition model. Purity Pu_m accounts for the enantiomeric enrichment of the membrane ultrafiltration step and indicates whether the process liquid can continue to the following steps or, instead, needs further enrichment. Recovery Re_m accounts for the performance of the membrane ultrafiltration step regarding the amount of enantiomer D obtained in the permeate in comparison with its initial amount in the feed. *PuRe* accounts for both the purity and recovery of enantiomer D, which allows for the use of one parameter for optimization. The objective is to find the highest *PuRe* value for the

membrane ultrafiltration step, which will strike a balance between obtaining a high purity and recovery.

3.1.2. Concentration and selective crystallization steps

Once sufficient enantioenrichment is obtained in the permeate for the enantiomer D, it is possible to selectively crystallize this enantiomer (Fig. 1). The three model amino acid systems are racemic compounds. Their ternary phase diagram represents the phase behavior of the mixture containing the solvent, enantiomer D, and enantiomer L; at a fixed temperature and pressure (Fig. 1c) [5,6]. Standard atmospheric pressure (101,325 Pa) is typically assumed for crystallization-based chiral resolution methods [5,6]. For racemic compounds, the ternary phase diagrams are characterized for having two symmetric eutectic points (Fig. 1c). A more detailed description about ternary phase diagrams of racemic compound-forming systems can be found in the literature [5,6,16]. In each eutectic point, a saturated liquid phase solution of the racemate is in equilibrium with the solid phases of the racemic compound and one of the pure enantiomers (D or L). Therefore, these points also distinguish the limits of the phase regions where we can find only one solid phase crystallizing (racemic compound or one enantiomer) (Fig. 1c). Our process focuses on the left side of the ternary phase diagram (Fig. 1c) because it is where the enantiomer D region lies down (Fig. 1c). The solvent-free enantiomer D fraction at the eutectic $x_{eu,D}$ indicates the enantiomeric ratio required to reach the eutectic equilibrium where both chiral solids coexist. Thus, the selective crystallization of the enantiopure product is only attainable as long as the enantiomeric enrichment level x_D reached surpasses the eutectic point composition $x_{eu,D}$ in the ternary phase diagram (Fig. 1c). So,

$$x_D > x_{eu,D} \tag{9}$$

Then, if the concentration in the permeate fulfills this boundary condition (9) so that x_D can be kept stable and above $x_{eu,D}$ under supersaturated conditions, the pure enantiomer can be crystallized (Fig. 1c).

We consider a cooling crystallization method for the last step of the process. However, the requirement of a concentration step (Fig. 1ac) between the membrane ultrafiltration and cooling crystallization steps is also studied.

For that, we define the concentration factor F:

$$F = \frac{C^*_{D,T}}{C_{D,p}} \tag{10}$$

which indicates how much the permeate concentration of enantiomer D $C_{D,p}$ needs to be concentrated to reach the solubility concentration $C^*_{D,T}$ of enantiomer D at temperature T in order to start the selective cooling crystallization step (Fig. 1c).

The crystallization step is assumed selective for only one of the two enantiomers (enantiomer D), meaning that the crystallization of the counter enantiomer L is prevented if the overall composition remains inside the two-phase region (where only the solid phase of enantiomer D can crystallize from the supersaturated liquid phase solution) of the ternary phase diagram during crystallization (Fig. 1c). The model considers that crystallization starts when the system is in this two-phase region of the ternary phase diagram (Fig. 1c) and that this point in the phase diagram will be maintained constant while the whole crystallization step takes place. This becomes feasible if we assume a steady-state condition that is given when operating in continuous mode.

The selective cooling crystallization starts at the saturation concentration $C^*_{D,T}$ of enantiomer D at temperature T and ends at the saturation concentration $C^*_{D,T'}$ of enantiomer D at temperature

T' (Fig. 1c). Then, only enantiomer D crystallizes out of the solution at *T'* (Fig. 1c), obtaining thus the enantiopure crystalline product (Fig. 1).

At this point, the model requires the definition of a fourth KPI, Re_c, the recovery in the selective cooling crystallization step:

1) Recovery of the selective crystallization step (Table 2)

$$Re_c = \frac{C^*_{D,T} - C^*_{D,T'}}{C^*_{D,T}} \tag{11}$$

The subscript *c* refers to the crystallization step. Here, crystallization volume V_c is assumed equal for both saturation concentrations $C^*_{D,T}$ and $C^*_{D,T'}$. Thus, Re_c assesses the amount of pure enantiomer crystals which can be collected from the crystallization step.

3.1.3. Overall process

A The racemic feed for the membrane ultrafiltration step renders an enantioenriched solution in the permeate (Fig. 1). Then, a concentration step between the membrane ultrafiltration and crystallization steps (Fig. 1ac) is required as the concentration in the permeate is low compared to the solubility of the enantiomer. Finally. if the enantioenriched permeate fulfills condition (9), the enantiomer can be selectively crystallized (Fig. 1).

We require a last KPI, Re_p, in order to account for the recovery of the overall process, which can be defined as follows:

1) Recovery of the overall process (Table 2)

$$Re_p = Re_m Re_c = \frac{V_c C^*_{D,T} - V_c C^*_{D,T'}}{V_0 C_{D,0}} \tag{12}$$

The subscript *p* refers to the overall process. The recovery Re_p compares the amount of pure enantiomer crystals obtained at the end of the process with the amount of the same enantiomer

in the feed. Note that the overall process recovery Re_p is the product of the recoveries of the membrane ultrafiltration and selective crystallization (Fig. 1).

Table 2. Model key performance indicators (KPIs) of the membrane-crystallization chiral resolution process.

KPI	Symbol	Mathematical definition	Equation
Membrane ultrafiltration purity	Pu_m	$Pu_m = \frac{C_{D,p}}{C_{D,p} + C_{L,p}}$	(5)
Membrane ultrafiltration recovery	Re_m	$Re_m = \frac{V_p C_{D,p}}{V_0 C_{D,0}}$	(6)
Membrane ultrafiltration *PuRe*	*PuRe*	$PuRe = (2Pu_m - 1)Re_m$	(7)
Selective crystallization recovery	Re_c	$Re_c = \frac{C^*_{D,T} - C^*_{D,T'}}{C^*_{D,T}}$	(11)
Overall process recovery	Re_p	$Re_p = \frac{V_c C^*_{D,T} - V_c C^*_{D,T'}}{V_0 C_{D,0}}$	(12)

3.2. Exploration of complexation conditions for the membrane ultrafiltration step

3.2.1. Speciation

The amino acid species concentrations evolve differently depending on the pH of the medium and the presence of the chiral selector BSA (Fig. 2). The concentrations of the different BSA species also depend on the pH because of the acid-base dissociation equilibrium with water (3) (Fig. 2a).

In the absence of chiral selector (Fig. 2bc left), the concentration profiles for enantiomers D and L species are the same when comparing each ionic species of the two enantiomers. This is found for the three amino acid systems phenylalanine, alanine, and valine (Fig. 2bc right). This means that both enantiomers have the same acid-base dissociation behavior when BSA is not present. Instead, when BSA is available (Fig. 2a and 2bc right), enantiomer D and L species concentration profiles are not the same anymore and differ from those with no chiral selector (Fig. 2bc). A maximum of complexation between the zwitterionic form of both enantiomers and chiral selector BSA is observed at pH = 9.3-9.5, where species $L^{\pm}$ binds more than $D^{\pm}$ to

the BSA (Fig. 2a), which is consistent with the larger value of the thermodynamic complexation constant K_L compared to K_D (Table 1). This different complexation behavior between both amino acid enantiomers can be exploited in the membrane ultrafiltration step and explains the enantiomeric enrichment that is obtained in the permeate, where the total concentration of the free enantiomer D species $C_{D,p}$ is higher than the total concentration of the free enantiomer L species $C_{L,p}$ (Fig. 2bc right).

a) BSA species (BSA presence, $C_{BSA,0}$ = 10^{-4} M)

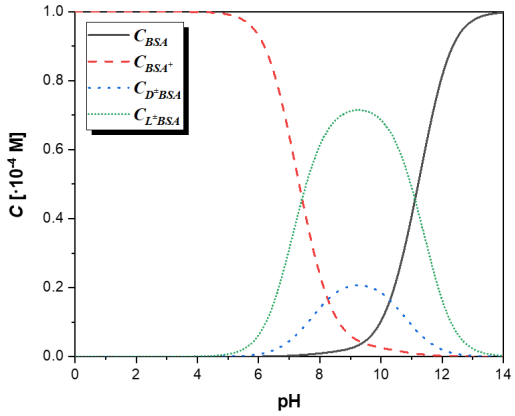

b) Free enantiomer D species (left: BSA absence, $C_{BSA,0}$ = 0 M; right: BSA presence, $C_{BSA,0}$ = 10^{-4} M)

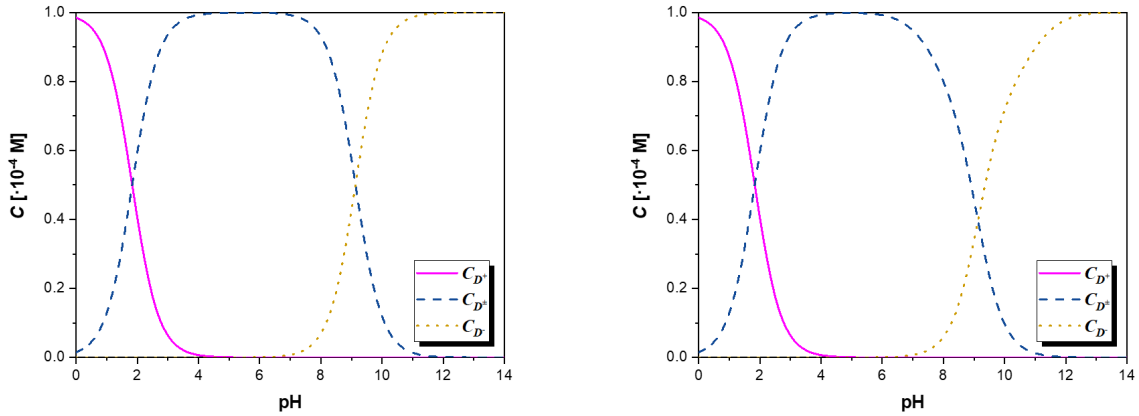

c) Free enantiomer L species (left: BSA absence, $C_{BSA,0}$ = 0 M; right: BSA presence, $C_{BSA,0}$ = 10^{-4} M)

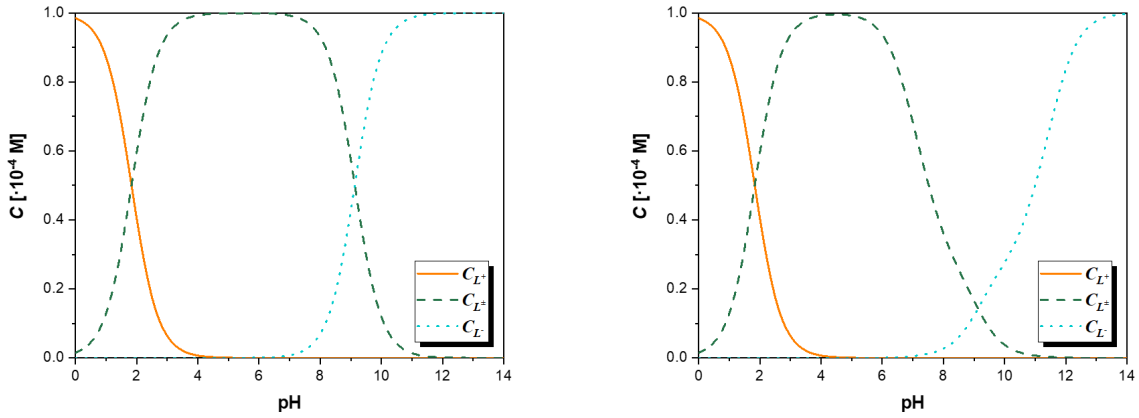

Fig. 2. Evolution of concentrations *C* of all the species involved in the complexation process, described by Eqs. (1)-(4), between the amino acids and chiral selector BSA: a) BSA species, b) free enantiomer D species, and c) free enantiomer L species. The simulations are for the phenylalanine system in absence of BSA with $C_{D,0} = C_{L,0} = 10^{-4}$ M and $C_{BSA,0} = 0$ M (b and c, left) and presence of BSA with $C_{D,0} = C_{L,0} = C_{BSA,0} = 10^{-4}$ M (a; b and c, right). Alanine and valine systems present similar concentration profiles.

3.2.2. Optimal complexation conditions

The model describing the complexation of the enantiomers of hydrophobic amino acids to the chiral selector BSA enables the exploration of process conditions to maximize purity Pu_m and recovery Re_m in the membrane ultrafiltration step. For that, Pu_m and Re_m equations are taken independently in a way that first the purity Pu_m equation is the objective function to be maximized for the one-site competition model, using Eqs. (1)-(6), and then after recovery Re_m is calculated for the optimal values obtained for purity Pu_m. The parameters for this optimization take the values of the thermodynamic constants provided in Table 1 and the fixed total amino acid enantiomer concentrations $C_{D,0} = C_{L,0} = 10^{-4}$ M. Then, the simulations reveal the maxima of purity Pu_m and their corresponding recovery Re_m in the BSA concentration range of $C_{BSA,0} = 10^{-8}$-10^{-1} M and pH range of pH = 0-14 (Fig. 3ab), based on the speciation dictated by the chemical equilibria (1)-(3). In practice, BSA concentrations $C_{BSA,0}$ would be fixed by dissolving the required amount of chiral selector BSA in the aqueous buffer solutions with the pH values required in each case. For these simulations' series, we assumed that the full initial volume V_0 fully converts into the permeate volume V_p, so the volume split ratio V_p/V_0 is equal to 1. This approach gives the same results when taking first recovery Re_m equation as the objective function to be maximized and after calculating purity Pu_m based on recovery Re_m optimal values. Thus, this means that the outcome of these simulations on purity Pu_m and recovery Re_m gives their maxima surfaces as a function of BSA concentration $C_{BSA,0}$ and pH ranges, as represented below (Fig. 3ab).

For the three amino acids under study (Phe, Ala, and Val), the same maxima are predicted due to the similar thermodynamic constants associated to their equilibria (Table 1). For the same initial concentrations of each enantiomer $C_{D,0} = C_{L,0} = 10^{-4}$ M, Pu_m maximum of 0.91 (Fig. 3a, in red) and Re_m maximum of 1.00 (Fig. 3b, in red) are obtained at different $C_{BSA,0}$ and pH values. Thus, it is observed that when the maximum of Pu_m is reached (Fig. 3a, in red) then, at the same $C_{BSA,0}$ and pH conditions, the minimum is obtained for Re_m (Fig. 3b, in blue). This is observed when $C_{BSA,0} \geq C_{D,0} = C_{L,0} = 10^{-4}$ M and pH = 9.3-9.5. This result agrees with the binding ratio of 1:1 between the zwitterionic form of one amino acid enantiomer and the unprotonated site in the chiral selector BSA, as the model proposes in Eq. (1). Therefore, the membrane process outcome is determined by the trade-off between the purity Pu_m and recovery Re_m in the membrane ultrafiltration step. Amino acid enantiomers concentrations $C_{D,0}$ and $C_{L,0}$ are chosen equal to 10^{-4} M based on the literature [32], indicating that the initial racemic solution concentration needs to be not very high to assume that the membrane ultrafiltration system does not present fouling phenomenon.

The trade-off observed makes desirable the optimization of the third KPI *PuRe*, which includes both purity Pu_m and recovery Re_m (Table 2), to determine the process conditions for the membrane ultrafiltration step at which the purity Pu_m is most balanced with the recovery Re_m. A U-type optimal *PuRe* surface is obtained in the pH-BSA concentration $C_{BSA,0}$ window at which *PuRe* has a value of around 0.40 for a wide range of combinations of pH and BSA concentration $C_{BSA,0}$. This optimal range corresponds to a value of purity Pu_m = 0.78 and recovery Re_m = 0.70 (Fig. 3c, light blue). Nevertheless, when considering the economics of the process, meaning using the least amount of chiral selector possible, since the use of it is costly, only one maximum appears, which is the one at $C_{BSA,0} = C_{D,0} = C_{L,0} = 10^{-4}$ M and pH = 9.3-9.5 (Fig. 3c, yellow circle). This maximum represents the optimal conditions to reach the enantioenriched permeate point for the membrane ultrafiltration step (Fig. 1c, grey point),

starting from the initial racemic feed (Fig. 1c, orange point). A *PuRe* value of 0.40 also indicates that there is still room for improvement until reaching the ideal *PuRe* = 1.00 (so, Pu_m = Re_m = 1.00). For that, two possibilities for improvement arise: trying to improve the current chemical system by a membrane cascade (see section 4.3.3.) or by improving the chemical system itself (see Appendix A).

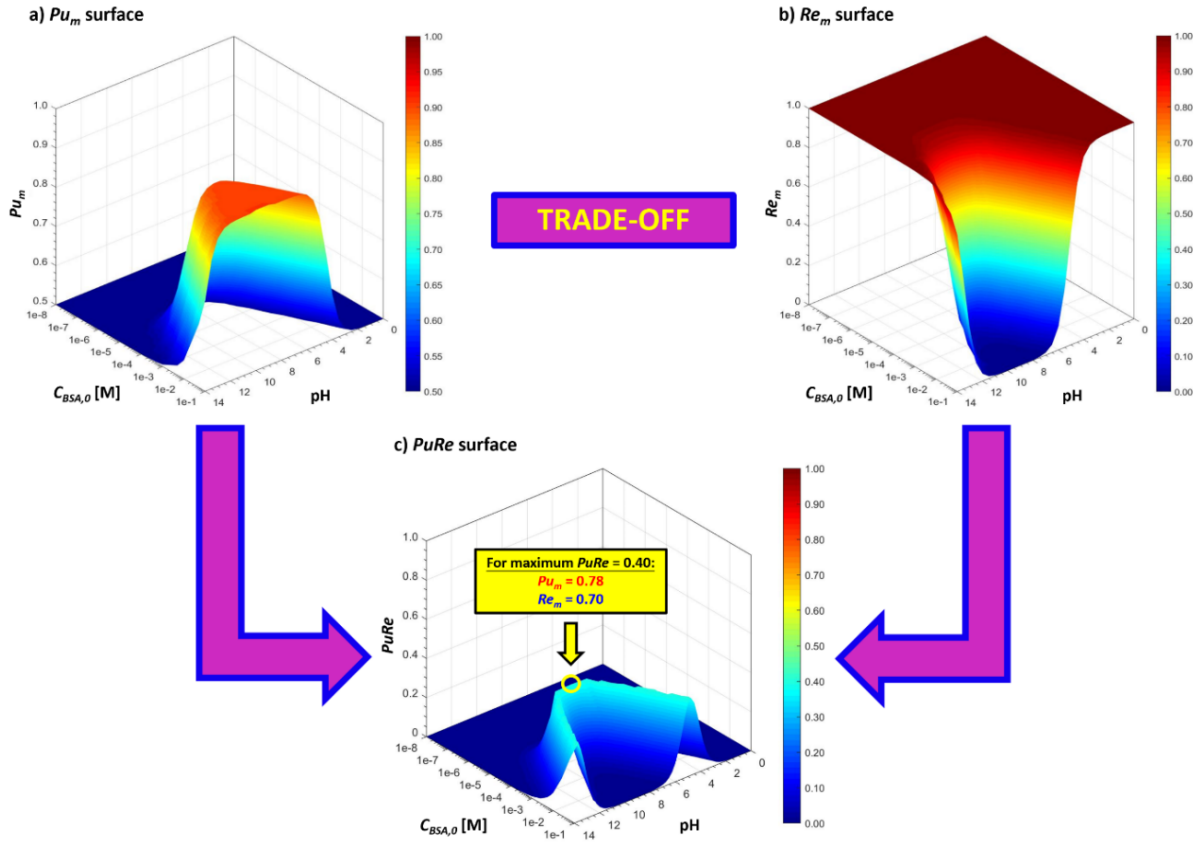

Fig. 3. a) Pu_m, b) Re_m, and c) *PuRe* surfaces as a function of BSA concentration $C_{BSA,0}$ and pH. There is a trade-off between Pu_m (a) and Re_m (b). The optimization of *PuRe* (c) indicates the best membrane ultrafiltration conditions (light blue region in the U-type surface in c) for the enantioenriched amino acid concentration, especially when considering the minimum use of BSA (yellow circle in c).

3.3. The need for a multi-stage membrane approach

Enantiopurity x_D data can be compared with the eutectic point composition $x_{eu,D}$, which is the limit that must be surpassed for the crystallization of the pure enantiomer (Table 3). The phenylalanine and alanine systems do not meet the condition $x_D > x_{eu,D}$ (9), whereas the valine

system does (Table 3). This means that D-valine could be separated with a single-stage membrane ultrafiltration crystallization process because the enantiomeric enriched point in the ternary phase diagram of valine (Fig. 1c, grey point) would already be inside the two-phase region (Fig. 1c, fuchsia point) where D-valine is the only solid that can crystallize after concentrating the permeate stream. On the contrary, phenylalanine and alanine would require a multi-stage membrane step to make the enantiomeric fraction x_D surpass their eutectic point compositions $x_{eu,D}$ (Table 3).

Table 3. Comparison of literature eutectic point composition $x_{eu,D}$ [33,34] with predicted enantiomeric purity x_D (here, equal to Pu_m) for the aqueous systems of amino acids Phe, Ala, and Val with chiral selector BSA, at 25ºC. Re_m and *PuRe* parameter values are also shown. *PuRe* value is obtained from its maximization in the one-site competition model, then Pu_m and Re_m values are related to this *PuRe* maximum.

System	Eutectic point composition, $x_{eu,D}$	x_D (Pu_m, model)	Re_m (model)	*PuRe* (model)
Phenylalanine	0.92			
Alanine	0.80	0.78	0.70	0.40
Valine	0.73			

A multi-stage membrane cascade approach (Fig. 4) is proposed in order to find the number of membrane stages n required to increase the solvent-free enantiomer fraction x_D.

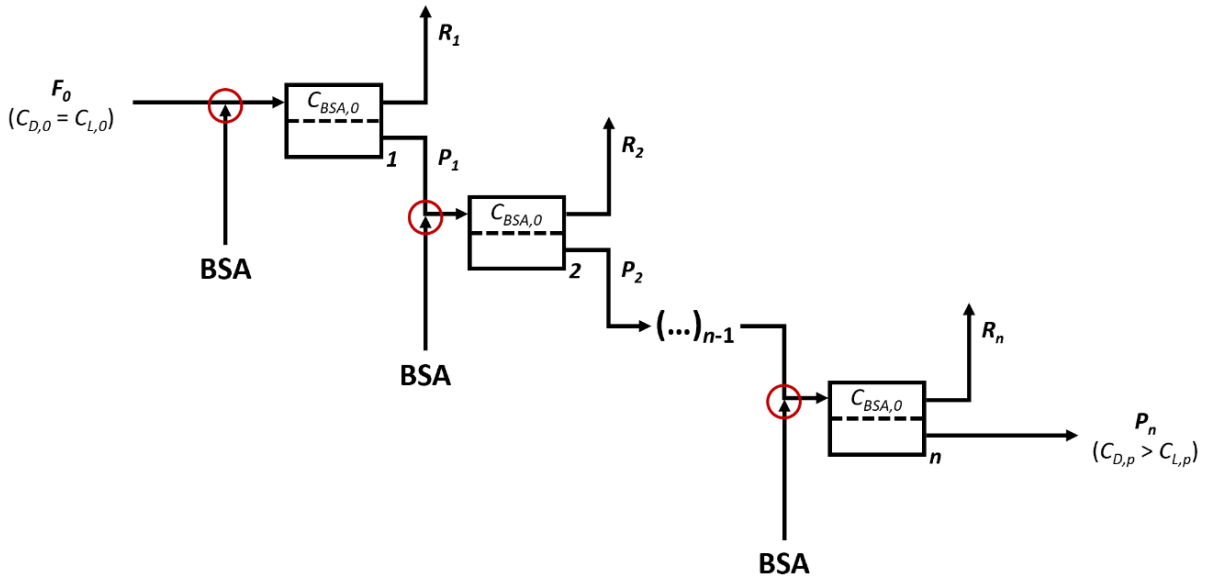

Fig. 4. A multi-stage membrane cascade for the membrane ultrafiltration step in order to enhance the enantiomeric enrichment. The feed F_0 consists of a racemic solution of amino acid to which is added a certain amount of BSA until reaching $C_{BSA,0}$. The equilibrated solution is filtered through the ultrafiltration membrane in stage 1, giving a permeate P_1 enriched with enantiomer D. The enriched permeate stream is fed into the next stage after fresh BSA is added. This process is repeated with n membrane stages until fulfilling $x_D > x_{eu,D}$ (9) in the permeate P_n. Retentates streams (R_1 to R_n) have the potential to be recycled in a further approach of the membrane cascade. So far, recycling is not considered in the simulations.

The retentate-permeate splitting effect studied relates the retentate volume V_r with the permeate volume V_p, which informs about how the feed volume V_0 is distributed to the retentate and permeate streams. Then, the retentate-permeate splitting can be seen as a parameter capable to inform about the membrane permeability (which is not explicitly included in our model) with a direct proportional relationship, and so with the effective membrane surface area. A splitting with higher fraction of permeate volume V_p indicates higher membrane permeability and/or effective membrane surface area. Contrarily, a splitting with lower permeate volume V_p proportion indicates lower membrane permeability and/or effective membrane surface area. Both number of membrane stages and splitting effects are studied in the outcome of the membrane ultrafiltration step (Pu_m and Re_m) for the three systems under study (Fig. 5). Phenylalanine, alanine, and valine systems show similar predicted purities when the number of membrane stages n and the retentate-permeate splitting effects are varied (Fig. 5). The main difference among these systems is the eutectic point composition $x_{eu,D}$ that phenylalanine, alanine, and valine require to surpass for the crystallization of the pure D-form (Table 3, Fig. 5 blue dotted line). Note that only the valine system meets the condition $x_D > x_{eu,D}$ (9) with a single membrane stage, as concluded earlier. The other two systems (Phe and Ala) require one more membrane stage to achieve such condition (9) (Fig. 5). Therefore, a 2-stage membrane ultrafiltration step for phenylalanine and alanine systems is needed for the feasible crystallization of their pure enantiomers. Note that the different retentate-permeate splitting,

that are related with the membrane permeability and/or effective membrane surface area, is predicted to have no effect on the purity obtained for the same membrane stage (Fig. 5). The recoveries of the three systems are different (Fig. 5). The predicted Re_m for valine will be higher than the ones for phenylalanine and alanine since the incorporation of an extra membrane stage translates to a decrease in Re_m (Fig. 5). Moreover, this change in the recovery will not only be affected by the number of membrane stages n but also by the retentate-permeate splitting. In addition, we observe that when the permeate volume V_p decreases to the detriment of the retentate volume V_r, then Re_m also decreases, even in the same membrane stage (Fig. 5).

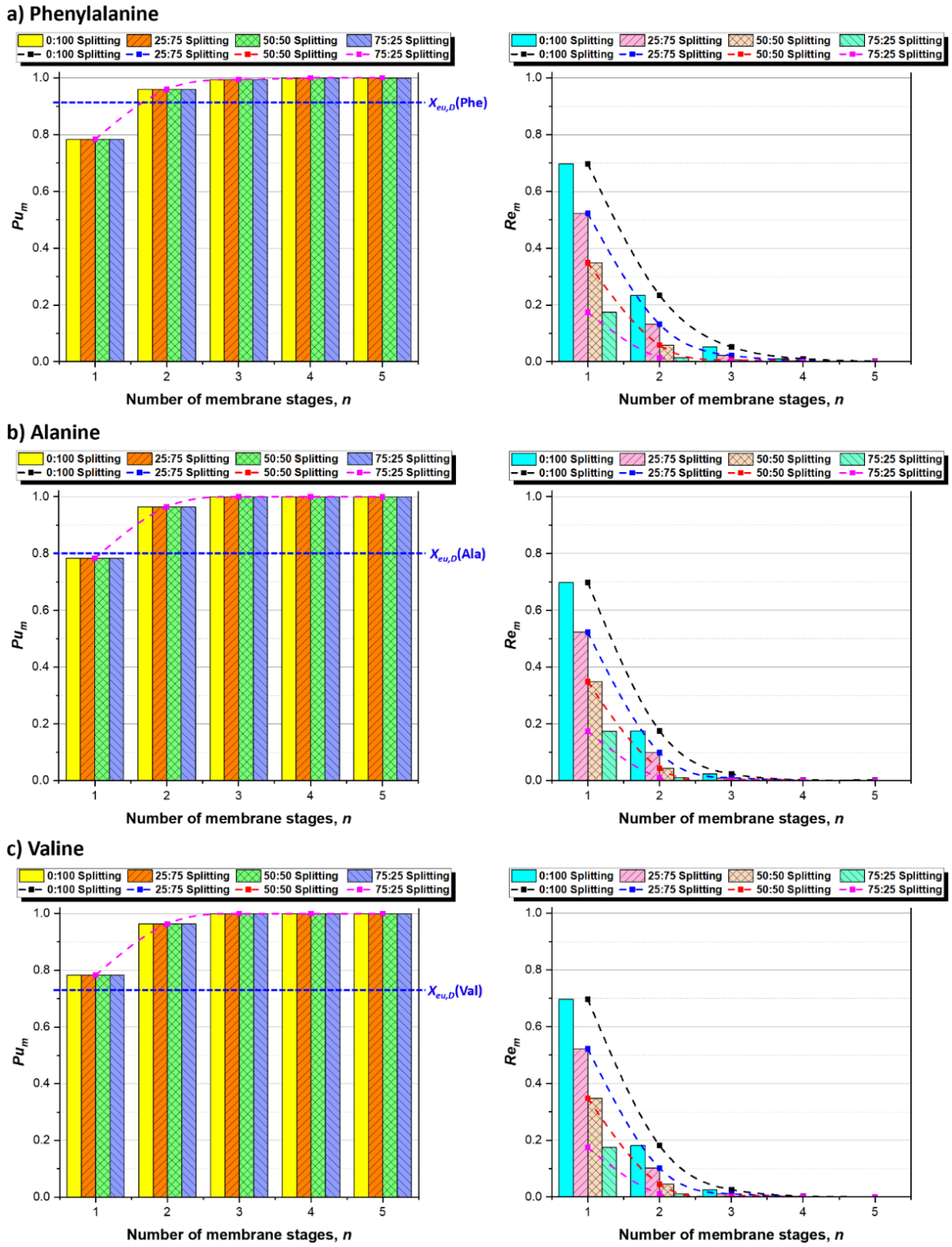

Fig. 5. Predicted Pu_m and Re_m obtained depending on the retentate-permeate splitting and number of membrane stages n applied in the membrane ultrafiltration step, for the three systems under study: a) phenylalanine, b) alanine, and c) valine. The blue dotted line in purity graphs represents the eutectic point composition $x_{eu,D}$ at 25ºC that each amino acid system requires to surpass to make feasible, in terms of purity, the crystallization of their pure D-form: a) $x_{eu,D}$(Phe) = 0.92, b) $x_{eu,D}$(Ala) = 0.80, and c) $x_{eu,D}$(Val) = 0.73.

3.4. Model validation

The results predicted from the one-site competition model for the membrane ultrafiltration step are validated for a single membrane stage. Several predicted amino acid enantiomers concentrations C_{pre} ($C_{D,p}$ and $C_{L,p}$) of phenylalanine are calculated using Eqs. (1)-(6) of the model and compared to the experimental C_{exp} values found in the literature (Fig. 6) [32].

The model predicts the experimental results better when the amino acid concentrations are low. A major discrepancy between prediction and experiments is observed when the concentrations are increasing (Fig. 6). At higher concentrations, only the D-form concentration is well predicted. The L-form shows higher calculated concentrations C_{pre} than the ones obtained in the experiments, C_{exp}. This last scenario seems to reflect a stronger interaction between the L-form and the chiral selector BSA at higher concentrations than the one predicted by their complexation constant in the model.

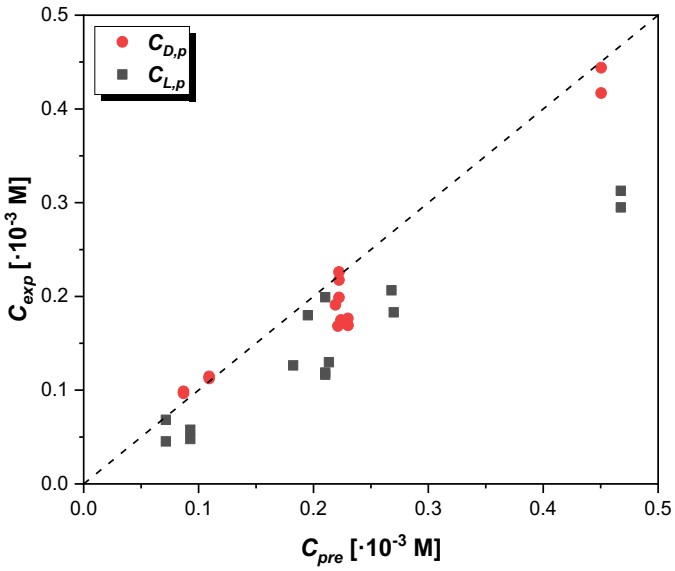

Fig. 6. Experimental permeate amino acid enantiomers concentrations C_{exp} (for Phe: $C_{D,p} = C_{L,p} = 0.3\text{-}5.0 \cdot 10^{-4}$ M) at a chiral selector concentration $C_{BSA,0} = 10^{-4}$ M in the pH range from 3 to 11 [32], versus their predicted concentration C_{pre} values calculated from the one-site competition model equations frame (see Eqs. (1)-(6)). The dashed line is just for comparison between experimental C_{exp} and predicted C_{pre} values.

3.5. Feasibility of the coupled crystallization step

Once the enantiomeric purity requirement is fulfilled, cooling crystallization can be applied just after the membrane ultrafiltration step or a concentration step may be needed first. Furthermore, the recovery for the overall process Re_p can be determined when the crystallization step is considered in the model.

The concentration and crystallization steps are assumed to be coupled to the membrane ultrafiltration step as represented in the phase diagram (Fig. 1c, fuchsia and yellow points). First, the permeate solution is concentrated from $C_{D,p}$ to $C^*_{D,T}$ and, then, this concentrate is cooled until reaching $C^*_{D,T'}$ to permit the crystallization of the D-form of the different amino acids considered (Phe, Ala, and Val). For this thermodynamic process, the following solubilities of the D-form of the amino acids studied were considered: $C^*_{D,T}$ = 56.4 (Phe), 292.9 (Ala), 78.3 mg·g^{-1} (Val) and $C^*_{D,T'}$ = 20.3 (Phe), 107.4 (Ala), and 49.5 mg·g^{-1} (Val). These solubilities were determined experimentally with the TV and EqC methods. Also, it is implied that only the D-form can crystallize because of meeting condition $x_D > x_{eu,D}$ (9) at the steady-state of the continuous process, as explained in section 4.3.1.2.

A concentration step is required between the membrane ultrafiltration and selective cooling crystallization steps. The concentration gap between the membrane ultrafiltration and crystallization steps is about 10^4-$2 \cdot 10^5$ times, when using the concentration levels reported in the literature for the membrane ultrafiltration step [32]. Specifically, the concentration factors F calculated with Eq. (10) are, from the highest to the lowest: $1.9 \cdot 10^5$ (Ala) > $1.5 \cdot 10^5$ (Phe) > $9.6 \cdot 10^4$ (Val), indicating a demanding process in terms of concentration process efficiency. The recoveries for each step Re_m and Re_c and for the overall process Re_p are illustrated below (Fig. 7) for different retentate-permeate splitting factors.

The membrane ultrafiltration recovery Re_m followed the same decreasing pattern with the retentate-permeate splitting ratio observed before (Fig. 5). The valine system has the highest Re_m value, then phenylalanine, and the lowest value is for alanine. The crystallization recovery Re_c does not depend on the retentate-permeate splitting and is higher for phenylalanine and alanine (both similar, ca. 65%) than valine system (ca. 40%). The overall process recovery Re_p decreases with the retentate-permeate splitting ratio and the highest value is predicted for valine, then phenylalanine, and the lowest value is predicted for the alanine system. Therefore, the splitting causes a decrease in Re_m, and then also in Re_p.

The highest overall process recoveries Re_p are expected for those systems that only require one membrane stage in the ultrafiltration step and have solubilities with strong temperature dependence. The number of membrane stages n seems more impactful than solubility, for temperature-dependent solubilities.

A coupled chiral resolution process consisting of a membrane ultrafiltration step followed by a concentration and selective cooling crystallization steps may be envisaged despite the concentration gap found for the systems investigated here.

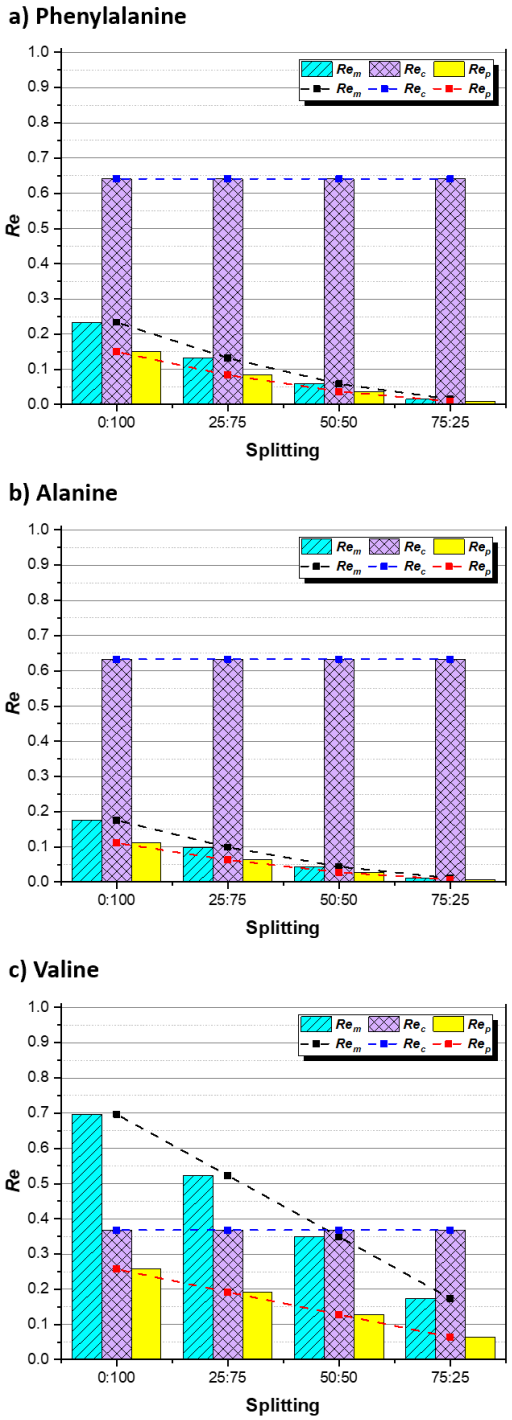

Fig. 7. Effect of retentate-permeate splitting on the predicted recoveries for the membrane ultrafiltration and crystallization steps (Re_m and Re_c, respectively) and overall process (Re_p) for the three amino acid systems under study: a) Phe, b) Ala, and c) Val.

4. Discussion

The process optimization of the membrane ultrafiltration step determines the best conditions to separate one enantiomer from the other as much as possible and, at the same time, obtaining the highest recovery Re_m possible for the desired enantiomer in the permeate. The optimization permits to find and treat the trade-off behavior between both purity Pu_m and recovery Re_m for the amino acids aqueous systems studied: phenylalanine, alanine, and valine. The one-site competition model predicts a maximum Pu_m and minimum Re_m for $C_{BSA,0} \geq C_{D,0} = C_{L,0} = 10^{-4}$ M and pH = 9.3-9.5, in agreement with the binding ratio of 1:1 between the zwitterionic form of one amino acid enantiomer and the unprotonated site in the chiral selector BSA, previously reported in the literature for tryptophan in water [13,14]. The optimization of *PuRe* and a process economics consideration predicts the optimal process conditions for the membrane ultrafiltration step at $C_{BSA,0} = C_{D,0} = C_{L,0} = 10^{-4}$ M and pH = 9.3-9.5 (Fig. 3c, yellow circle).

The model predicts a single-stage membrane ultrafiltration for valine in terms of enantiopurity x_D. However, it predicts at least one stage more for the other two systems phenylalanine and alanine in order to meet condition $x_D > x_{eu,D}$ (9) for the crystallization of a pure enantiomer (Fig. 5). For all the systems, the Pu_m obtained is very similar showing no differences with retentate-permeate splitting ratio and following the same pattern with the number of membrane stages n. The last fact occurs because of taking the same complexation constants (pK_D and pK_L) for phenylalanine as for alanine and valine calculations, assuming that hydrophobic amino acids with similar structure should have similar interactions with the same chiral selector. In that way, Pu_m is expected to change more when systems are more different between them, that is, having different interaction affinities with the chiral selector. The model predicts higher Re_m in valine than in phenylalanine and alanine due to the incorporation of an extra membrane stage, fact seen as the trigger for the decrease in Re_m.

The membrane ultrafiltration model, validated with experimental data obtained from the literature for phenylalanine system [32], predicts better results at low concentrations. At higher concentrations, D-form concentration is adjusted to its prediction, whereas L-form shows higher predicted concentrations values than the ones obtained in the experiments (Fig. 6). This fact seems to reflect a stronger interaction between L-form and BSA at higher concentrations. This observation can be of utility for the refinement of equilibria complexation constants, a procedure that might help to predict or give a more accurate estimation of these thermodynamic constants in accordance to experiments.

The complexation and chiral selector acid-base dissociation constants sensitivity studies (Figs. A.1-A.4) not only confirmed the modeled behavior reported [13,14], but also affirmed that an ideal BSA-similar chiral selector should bear an unprotonated binding site for a large pH range and very different complexation constants for each enantiomer, meaning that a $\left| \mathrm{p}K_D - \mathrm{p}K_L \right| \geq$ 2-3. These are the main chiral selector properties that will make possible the obtaining of sufficient enantiomeric enrichment with also enough recovery in the membrane ultrafiltration step. Furthermore, we believe that the type of sensitivity studies shown can be useful even when considering BSA-different chiral selectors. For them, new parameters and values might be required, but the importance of assessing the KPIs (Table 2) in the way we describe here will permit researchers to optimize the chiral selectivity conditions in the process, which are tightly linked to the overall process outcome. We also think that molecular docking and molecular dynamics simulations would be helpful tools for the major understanding of the fit between the enantiomers and chiral selector systems which require molecular interaction specificity.

The feasibility study for the coupling of the cooling crystallization step confirms that a concentration step (e.g. distillation or simple evaporation) is required between the membrane ultrafiltration and the crystallization steps. The concentration factors *F* for the three amino acid

systems investigated (Phe, Ala, and Val) are found high, indicating a demanding process in terms of concentration process efficiency. However, when analyzing the recoveries for the membrane ultrafiltration Re_m and crystallization Re_c steps as well as for the overall process Re_p, we can infer that, when saving the concentration step is possible or this is small, this process in a whole could become feasible and be able to produce good recoveries for those systems that only require one membrane stage in the ultrafiltration step and have solubilities with a strong temperature dependence.

We envisage that the overall process recovery Re_p can be increased when applying the recycling step in the process (Fig. 8a). This new step can be easily understood as the introduction of a recycled enantioenriched solution which includes: the retentate (or retentates, if several membrane stages apply) in the membrane ultrafiltration step, the pure solvent from the concentration step, and the enantioenriched remaining solution from the selective crystallization step. This is shown in the overall process represented in the ternary phase diagram (Fig. 8b, green and white points). Note that the model and simulations presented here assume the introduction of fresh free chiral selector at each stage of the membrane ultrafiltration step (Fig. 4). However, we think that the recyclability of the complexed form of the chiral selector should be considered to make the process more cost-effective. This could be achieved by recuperating the original free form of the chiral selector by readjusting the pH conditions in such a way that the enantiomers could be unbound from the chiral selector.

Finally, the coupled process described is restricted to the existing interaction between the chiral selector and the racemic compounds examined. In the future, we aim at testing the new combined resolution process with other BSA-similar/different chiral selectors and for other racemic compounds in not only aqueous media but also in organic solvents or in their mixtures with water. In addition, apart from a cooling crystallization, other types of crystallization

techniques could be assessed depending on the solubility behavior of the enantiopure product of interest.

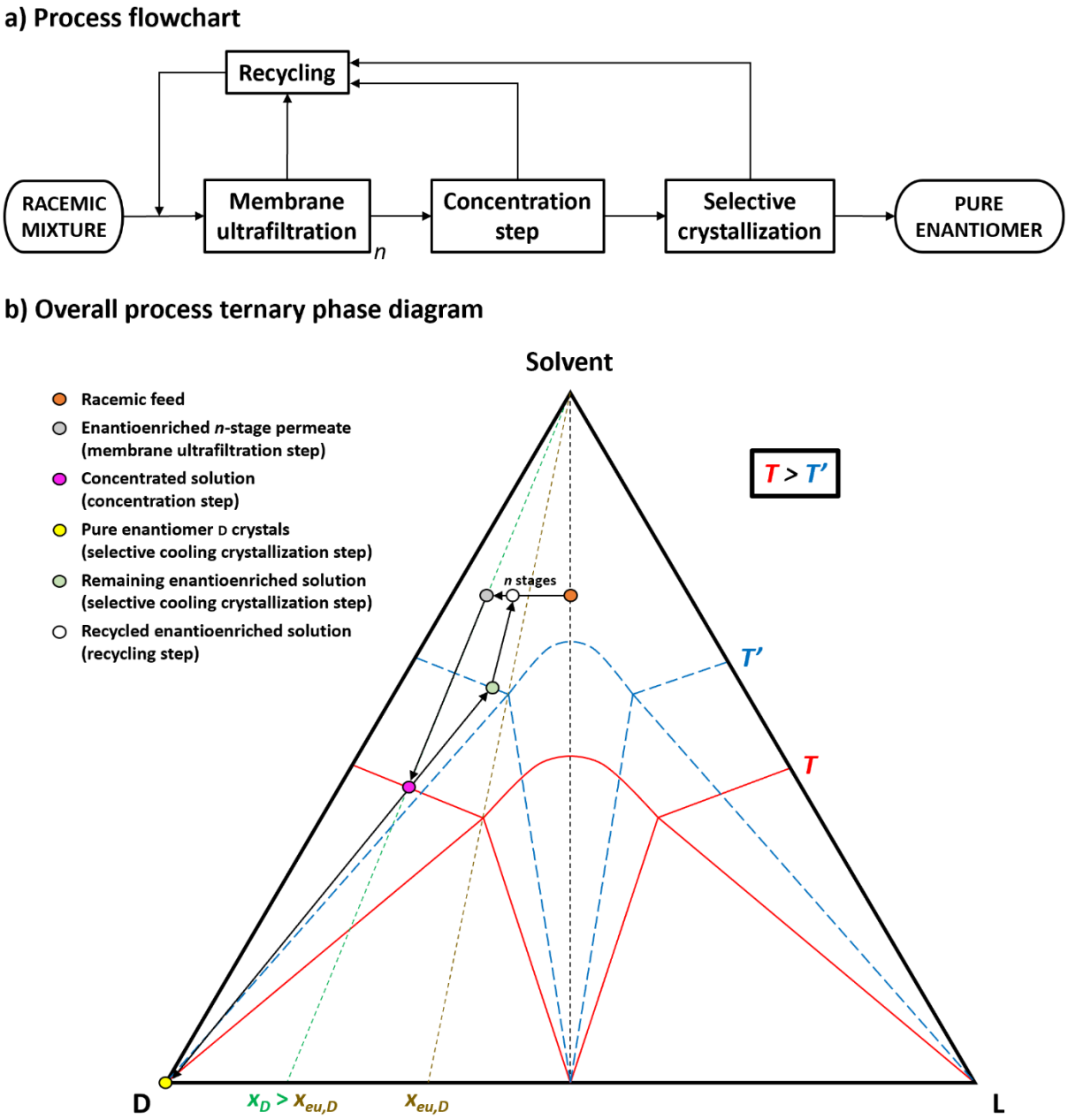

Fig. 8. a) Process flowchart starting from an equilibrated racemic mixture (feed) until the obtaining of a pure enantiomer and b) overall process ternary phase diagram for the resolution of a racemic compound-forming system, now completed with the recycling step.

5. Conclusions

The one-site competition model is well applicable to describe the complexation interaction between the chiral selector BSA and the hydrophobic amino acids phenylalanine, alanine, and valine in aqueous media. In the membrane ultrafiltration step, a trade-off exists between the purity and recovery in the permeate because the same complexation conditions that favored purity also favored the binding of both competing enantiomers to BSA due to the partial stereoselectivity of this chiral selector with the three amino acid systems. Although with different binding proportion of both enantiomers to BSA, the recovery decreases. The conditions to obtain the optimal purity and recovery correspond to $C_{BSA,0} = C_{D,0} = C_{L,0}$, based on the minimum use of BSA in view of its high cost, and pH = 9.3-9.5. The model predicts that, starting from a racemic solution, a single-stage membrane ultrafiltration can lead to a purity that is enriched sufficiently beyond the eutectic point composition for the valine system to enable, after a concentration step, the continuous crystallization of the pure enantiomer solid product. However, for those systems with a more demanding eutectic point composition, such as phenylalanine and alanine, more membrane stages are needed. The sensitivity studies for the complexation and chiral selector acid-base dissociation constants predict that an optimal chiral selector similar to BSA should bear an unprotonated binding site for a large pH range, so a low pK_{BSA}, and highly distinct complexation constants for the two enantiomers with $\left| pK_D - pK_L \right|$ equal or larger than 2. The overall process obtains the optimal recovery when the concentration gap between the membrane ultrafiltration and crystallization steps is saved or small and for those systems which only require one membrane stage in the ultrafiltration step and have solubilities with a strong temperature dependence. We envisage that the sensitivity study of other chiral selectors and its optimization in a similar way as described here along with the introduction of a recycling step, which will recirculate a partial enantioenriched solution into the process, will increase the overall process recovery not only for the systems investigated

here, but also for other chiral systems. Therefore, this novel membrane ultrafiltration-crystallization resolution process has application potential for the enantioseparation of racemic solutions of racemic compound-forming systems.

Declaration of competing interest

The authors declare that they have no known competing financial interests or personal relationships that could have appeared to influence the work reported in this paper.

Notation

Ala	Alanine
BSA	Bovine serum albumin
C	Concentration [M]
C_{BSA}	Concentration of chiral selector BSA with unprotonated complexation site [M]
C_{BSA+}	Concentration of chiral selector BSA^+ with protonated complexation site [M]
$C_{BSA,0}$	Total (feed/initial) concentration of chiral selector BSA [M]
C_{D+}	Concentration of cation D^+ (amino group protonated) [M]
$C_{D\pm}$	Concentration of zwitterion $D^\pm$ (amino group protonated and carboxyl group deprotonated) [M]
C_{D-}	Concentration of anion D^- (carboxyl group deprotonated) [M]
$C_{D\pm BSA}$	Concentration of complex $D^\pm$BSA [M]
$C_{D,p}$	Total concentration of enantiomer D (all free species) in permeate [M]
$C_{D,r}$	Total concentration of enantiomer D (just free species) in retentate [M]
$C_{D,0}$	Total (feed/initial) concentration of enantiomer D [M]
$C^*_{D,T}$	Solubility concentration for enantiomer D at temperature T [mg·g^{-1}]
$C^*_{D,T'}$	Solubility concentration for enantiomer D at temperature T' [mg·g^{-1}]
C_{exp}	Experimental concentration [M]
C_{L+}	Concentration of cation L^+ (amino group protonated) [M]
$C_{L\pm}$	Concentration of zwitterion $L^\pm$ (amino group protonated and carboxyl group deprotonated) [M]
C_{L-}	Concentration of anion L^- (carboxyl group deprotonated) [M]
$C_{L\pm BSA}$	Concentration of complex $L^\pm$BSA [M]
$C_{L,p}$	Total concentration of enantiomer L (all free species) in permeate [M]

$C_{L,r}$ Total concentration of enantiomer L (just free species) in retentate [M]

$C_{L,0}$ Total (feed/initial) concentration of enantiomer L [M]

C_{pre} Predicted concentration [M]

C_w Concentration of H_2O [M]

C_{w+} Concentration of H_3O^+ [M]

$C_{x,0}$ Total (feed/initial) concentration of species *x* [M]

$E_{D,p}$ Enantiomeric excess of enantiomer D in the permeate [-]

EqC Equilibrium concentration method

F_0 Feed stream

F Concentration factor [-]

$K_{a1,D}$ Dissociation constant of the first proton of enantiomer D [-]

$K_{a2,D}$ Dissociation constant of the second proton of enantiomer D [-]

$K_{a1,L}$ Dissociation constant of the first proton of enantiomer L [-]

$K_{a2,L}$ Dissociation constant of the second proton of enantiomer L [-]

K_{BSA} Dissociation constant of proton of chiral selector BSA complexation site [-]

K_D Complexation constant of enantiomer D and chiral selector BSA [-]

K_L Complexation constant of enantiomer L and chiral selector BSA [-]

KPI Key performance indicator

n Number of membrane ultrafiltration stages [stage or stages]

Phe Phenylalanine

P_n Permeate stream of stage *n* of the membrane ultrafiltration step

Pu_m Purity of the membrane ultrafiltration step [-]

PuRe PuRe of the membrane ultrafiltration step [-]

R_n Retentate stream of stage *n* of the membrane ultrafiltration step

Re_c Recovery of the crystallization step [-]

Re_m Recovery of the membrane ultrafiltration step [-]

Re_p Recovery of the overall process [-]

RSD Relative standard deviation [%]

T Initial temperature for the cooling crystallization step [ºC]

T' Ending temperature for the cooling crystallization step [ºC]

Trp Tryptophan

TV Temperature variation method

V_0 Feed (initial) volume [L]

Val Valine

V_c Crystallization volume [L]

V_p Permeate volume [L]

V_r Retentate volume [L]

x_D Solvent-free enantiomer fraction for enantiomer D [-]

$x_{eu,D}$ Enantiomeric ratio in the eutectic point (also referred as eutectic point composition) for enantiomer D [-]

x_L Solvent-free enantiomer fraction for enantiomer L [-]

Acknowledgements

Jose Capdevila-Echeverria thanks for the hospitality he enjoyed during his research visit to Prof. Richard Lakerveld's laboratory in the Department of Chemical and Biological Engineering at The Hong Kong University of Science and Technology. Jiayuan Wang is grateful for the warm welcome experienced during his research visit to Prof. Joop H. ter Horst's research group at the CMAC Future Manufacturing Research Hub at the University of Strathclyde. The authors would like to thank Carlos Moreno-Leon for carefully reading the manuscript. This work was funded by the International Strategic Partnership between University of Strathclyde and Nanyang Technological University Singapore and the Future Continuous Manufacturing and Advanced Crystallisation Research Hub (grant ref.: EP/P006965/1). The authors would like to acknowledge that part of the work was carried out in the CMAC National Facility supported by UKRPIF (UK Research Partnership Fund) award from the Higher Education Funding Council for England (HEFCE) (grant ref.: HH13054).

References

[1] J.E. Rekoske, Chiral separations, AIChE J. 47 (2001) 2–5.

[2] N. Chhabra, M. Aseri, D. Padmanabhan, A review of drug isomerism and its significance, Int. J. Appl. Basic Med. Res. 3 (2013) 16–18.

[3] W.H. Pirkle, C.J. Welch, An improved chiral stationary phase for the chromatographic separation of underivatized naproxen enantiomers, J. Liq. Chromatogr. 15 (1992) 1947–1955.

[4] Y. Yang, B. Su, Q. Yan, Q. Ren, Separation of naproxen enantiomers by supercritical/subcritical fluid chromatography, J. Pharm. Biomed. Anal. 39 (2005) 815–818.

[5] J. Jacques, A. Collet, Enantiomers, racemates and resolutions, John Wiley & Sons, 1981.

[6] H. Lorenz, A. Seidel-Morgenstern, Processes to separate enantiomers, Angew. Chemie - Int. Ed. 53 (2014) 1218–1250.

[7] S. Mane, Racemic drug resolution: a comprehensive guide, Anal. Methods. 8 (2016) 7567–7586.

[8] I. Ali, V.K. Gupta, H.Y. Aboul-Enein, Chiral resolution of racemic environmental pollutants by capillary electrophoresis, Crit. Rev. Anal. Chem. 38 (2008) 132–146.

[9] R. Kallenborn, H. Hühnerfuss, Chiral environmental pollutants: trace analysis and ecotoxicology, Springer, 2010.

[10] A.A. Basheer, Chemical chiral pollution: impact on the society and science and need of the regulations in the 21st century, Chirality. 30 (2018) 402–406.

[11] R. Xie, L.-Y. Chu, J.-G. Deng, Membranes and membrane processes for chiral resolution, Chem. Soc. Rev. 37 (2008) 1243–1263.

[12] S. Poncet, J. Randon, J.L. Rocca, Enantiomeric separation of tryptophan by ultrafiltration using the BSA solution system, Sep. Sci. Technol. 32 (1997) 2029–2038.

[13] F. Garnier, J. Randon, J.L. Rocca, Enantiomeric separation by ultrafiltration: complexation mechanism of tryptophan analogs to bovine serum albumin, Sep. Purif. Technol. 16 (1999) 243–250.

[14] J. Randon, F. Garnier, J.L. Rocca, B. Maïsterrena, Optimization of the enantiomeric separation of tryptophan analogs by membrane processes, J. Memb. Sci. 175 (2000) 111–117.

[15] H. Lorenz, A. Perlberg, D. Sapoundjiev, M.P. Elsner, A. Seidel-Morgenstern, Crystallization of enantiomers, Chem. Eng. Process. Process Intensif. 45 (2006) 863–873.

[16] H. Lorenz, D. Sapoundjiev, A. Seidel-Morgenstern, Solubility equilibria in chiral systems and their importance for enantioseparation, Eng. Life Sci. 3 (2003) 132–136.

[17] J.H. ter Horst, C. Schmidt, J. Ulrich, Fundamentals of industrial crystallization, in: Handb. Cryst. Growth Bulk Cryst. Growth Second Ed., 2014: pp. 1317–1349.

[18] S. Srisanga, J.H. Ter Horst, Racemic compound, conglomerate, or solid solution: phase diagram screening of chiral compounds, Cryst. Growth Des. 10 (2010) 1808–1812.

[19] L.C. Sögütoglu, R.R.E. Steendam, H. Meekes, E. Vlieg, F.P.J.T. Rutjes, Viedma ripening: a reliable crystallisation method to reach single chirality, Chem. Soc. Rev. 44 (2015) 6723–6732.

[20] L. Gou, S. Robl, K. Leonhard, H. Lorenz, M. Sordo, A. Butka, S. Kesselheim, M. Wolff, A. Seidel-Morgenstern, K. Schaber, A hybrid process for chiral separation of compound-forming systems, Chirality. 23 (2011) 118–127.

[21] S. Robl, L. Gou, A. Gere, M. Sordo, H. Lorenz, A. Mayer, C. Pauls, K. Leonhard, A. Bardow, A. Seidel-Morgenstern, K. Schaber, Chiral separation by combining pertraction and preferential crystallization, Chem. Eng. Process. Process Intensif. 67 (2013) 80–88.

[22] H. Kaemmerer, Z. Horvath, J.W. Lee, M. Kaspereit, R. Arnell, M. Hedberg, B. Herschend, M.J. Jones, K. Larson, H. Lorenz, A. Seidel-Morgensten, Separation of racemic bicalutamide by an optimized combination of continuous chromatography and selective crystallization, Org. Process Res. Dev. 16 (2012) 331–342.

[23] J. von Langermann, M. Kaspereit, M. Shakeri, H. Lorenz, M. Hedberg, M.J. Jones, K. Larson, R. Herschend, R. Arnell, E. Temmel, J.-E. Ba, A. Kienle, A. Seidel-Morgenstern, Design of an integrated process of chromatography, crystallization and racemization for the resolution of 2′,6′-pipecoloxylidide (PPX), Org. Process Res. Dev. 16 (2012) 343–352.

[24] M.A. Reus, A.E.D.M. van der Heijden, J.H. ter Horst, Solubility determination from clear points upon solvent addition, Org. Process Res. Dev. 19 (2015) 1004–1011.

[25] GAMS Software GmbH, GAMS, (2019). https://www.gams.com/ (accessed August 5, 2019).

[26] GAMS Software GmbH, GAMS solver manual, (2020). https://www.gams.com/latest/docs/S_MAIN.html (accessed May 21, 2020).

[27] TheMathWorks, MATLAB, (2019). https://uk.mathworks.com/?s_tid=gn_logo (accessed August 5, 2019).

[28] S. Dirkse, M.C. Ferris, J. Ramakrishnan, GDXMRW: interfacing GAMS and MATLAB, (2014). https://www.gams.com/latest/docs/T_GDXMRW.html (accessed August 5, 2019).

[29] A. Higuchi, T. Hashimoto, M. Yonehara, N. Kubota, K. Watanabe, S. Uemiya, T. Kojima, M. Hara, Effect of surfactant agents and lipids on optical resolution of amino acid by ultrafiltration membranes containing bovine serum albumin, J. Memb. Sci. 130 (1997) 31–39.

[30] F.A. Carey, R.M. Giuliano, Organic chemistry, 10th ed., McGraw-Hill Education, New York, 2016.

[31] J. Romero, A.L. Zydney, Staging of affinity ultrafiltration processes for chiral separations, J. Memb. Sci. 209 (2002) 107–119.

[32] J. Tian, M. Pan, Y. Ma, J.W. Chew, Effect of membrane fouling on chiral separation, J. Memb. Sci. 593 (2019) 117352.

[33] M. Klussmann, H. Iwamura, S.P. Mathew, D.H. Wells, U. Pandya, A. Armstrong, D.G. Blackmond, Thermodynamic control of asymmetric amplification in amino acid catalysis, Nature. 441 (2006) 621–623.

[34] M. Klussmann, A.J.P. White, A. Armstrong, D.G. Blackmond, Rationalization and prediction of solution enantiomeric excess in ternary phase systems, Angew. Chemie - Int. Ed. 45 (2006) 7985–7989.